REF: A0604.0029 *(Invited Paper)*

A NEW METHODOLOGY FOR THE CHARACTERIZATION OF MODE II FRACTURE OF PINUS PINASTER WOOD

M.F.S.F. de Moura[1*], M.A.L. Silva[2], J.J.L. Morais[2], A.B. de Morais[3], and J. L. Lousada[4]
[1]Faculdade de Engenharia, Universidade do Porto, Portugal
[2]CETAV/UTAD, Departamento de Engenharias, Vila Real, Portugal
[3]Universidade de Aveiro, Dep. de Eng. Mecânca, Aveiro, Portugal
[4]UTAD, Departamento de Florestal, Vila Real, Portugal
Email: (*)mfmoura@fe.up.pt

SYNOPSIS

In this study, the End Notched Flexure (ENF) fracture test was used to obtain the mode II *R*-curve of the *Pinus pinaster* wood in the RL crack propagation system. The test method was numerically and experimentally analyzed. In the numerical study, three (3D) and two-dimensional (2D) finite element analyses were conducted to determine the mode II critical strain energy release rate (G_{IIc}) and the respective *R*-curve. Firstly, the 3D analysis was performed in order to obtain the strain energy release rates distributions at the crack tip, and consequently, to identify the presence of spurious fracture modes that could affect the measured G_{IIc}. The *P*-δ-*a* values determined from the 3D model were compared with the same values obtained from the 2D model. The main objective was to validate the 2D model, which is computationally less expensive. On the other hand, measurement of the crack length in the ENF test is quite difficult in wood because crack tends to close during propagation. To avoid this experimental problem a Compliance-Based Beam Method (CBBM), based on equivalent crack approach, is proposed. Moreover, this method does not require additional experimental tests to obtain the elastic properties. Experimental tests were also executed in order to verify the numerical results. The aim is to introduce the CBBM as a standard data reduction scheme in order to measure the G_{IIc} value.

INTRODUCTION

Wood is a widely used engineering material with notable mechanical properties in spit of its low density. The mechanical behaviour of wood is strongly affected by the complex anatomy of this material. In fact, properties like stiffness and strength are much influenced by the wood internal structure. Macroscopically, wood can be considered a cylindrically orthotropic material, with three symmetry material directions (L, R and T). The longitudinal direction (L) is parallel to stem axis, the radial direction (R) is perpendicular to the growth rings and the tangential direction (T) is tangential to them. For a complete characterization of wood fracture behaviour it is necessary to study six crack propagation systems. These propagation systems are usually represented by two letters: the first one represents the direction perpendicular to the crack plane and the second one indicates the direction of crack propagation. One of the most frequent crack propagation systems is the RL one which was studied in this work. The mode I fracture has been widely studied and the Double Cantilever Beam (DCB) test is frequently used to identify the mode I fracture properties (Morel, 2003; Jensen, 2005 and Yoshihara, 2006). Nowadays, there is a significant interest on the determination of the mode II critical strain energy release rate (G_{IIc}). In wood, two test configurations have been proposed: the End Notched Flexure (ENF) (Barrett, 1977; Yoshihara, 2000 and de Moura,

2006) and the Four Point End Notched Flexure (4ENF) (Yoshihara, 2004). Due to its simplicity the ENF configuration is the most appealing test to determine the mode II fracture properties of wood. However, there are two important difficulties to be solved before it can be accepted as a standard test for mode II fracture characterization of wood. The first one is the difficulty inherent to crack monitoring during propagation, which can induce non negligible errors on the derivative of the compliance relatively to the crack length (dC/da). On the other hand, the wood heterogeneity leads to significant specimen-to-specimen variation of the Young´s modulus, which implies its measurement before performing the ENF tests. To overcome these problems, a new data reduction scheme based on specimen compliance and on equivalent crack length approach is proposed. The method is initially validated numerically and applied to experimental data in order to obtain the G_{IIc} value of a *Pinus pinaster* wood.

NUMERICAL ANALYSIS

The ENF specimen geometry adopted in this study is presented in figure 1. The specimen dimensions ($2h$=20 mm, L=230 mm, L_1=250 mm, B=20 mm and a_0=162 mm) were chosen according to relations presented in (Caumes, 1987). Table 1 presents the nominal elastic and fracture properties of the *Pinus pinaster* wood.

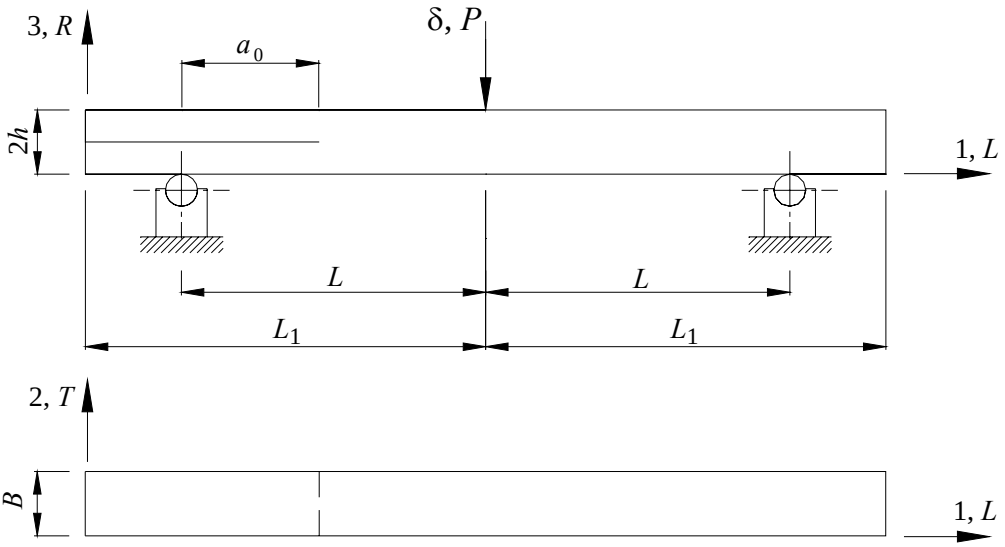

Fig. 1 The ENF specimen geometry.

Table 1. Nominal elastic and fracture properties of the Pinus pinaster wood (de Moura, 2006).

E_L (GPa)	E_R (GPa)	E_T (GPa)	υ_{LR}	υ_{TL}	υ_{RT}	G_{LR} (GPa)	G_{TL} (GPa)	G_{RT} (GPa)
15.13	1.91	1.01	0.47	0.51	0.59	1.12	1.04	0.17

σ_L^{ult} (MPa)	σ_R^{ult} (MPa)	σ_T^{ult} (MPa)	τ_{LR}^{ult} (MPa)	τ_{LT}^{ult} (MPa)	G_{IIc} (N/mm)
97.46	7.93	4.20	16.0	16.0	0.63

In order to simulate damage initiation and propagation a cohesive mixed-mode damage model based on interface finite elements was considered. A constitutive relationship between the vectors of stresses ($\boldsymbol{\sigma}$) and relative displacements ($\boldsymbol{\delta}$) is established. The method requires local strengths ($\sigma_{u,i}$, i=I, II, III) and the critical strain energies release rates (G_{ic}) as inputted data parameters. Damage onset is predicted using a quadratic stress criterion

$$\begin{aligned} &\left(\frac{\sigma_{\mathrm{I}}}{\sigma_{u,\mathrm{I}}}\right)^2+\left(\frac{\sigma_{\mathrm{II}}}{\sigma_{u,\mathrm{II}}}\right)^2+\left(\frac{\sigma_{\mathrm{III}}}{\sigma_{u,\mathrm{III}}}\right)^2=1 \quad \text{if} \quad \sigma_{\mathrm{I}}\geq 0 \\ &\left(\frac{\sigma_{\mathrm{II}}}{\sigma_{u,\mathrm{II}}}\right)^2+\left(\frac{\sigma_{\mathrm{III}}}{\sigma_{u,\mathrm{III}}}\right)^2=1 \qquad \text{if} \quad \sigma_{\mathrm{I}}\leq 0 \end{aligned} \tag{1}$$

where σ_i, (i=I, II, III) represent the stresses in each mode. Crack propagation was simulated by a linear energetic criterion

$$\frac{G_{\mathrm{I}}}{G_{\mathrm{Ic}}}+\frac{G_{\mathrm{II}}}{G_{\mathrm{IIc}}}+\frac{G_{\mathrm{III}}}{G_{\mathrm{IIIc}}}=1\ . \tag{2}$$

Basically, it is assumed that the area under the minor triangle of figure 2 represents the energy released in each mode, which is compared to the respective critical fracture energy represented by the bigger triangle. The subscripts o and u refer to onset and ultimate relative displacement and the subscript m states for mixed-mode case. More details about the used model are presented in (de Moura, 2006).

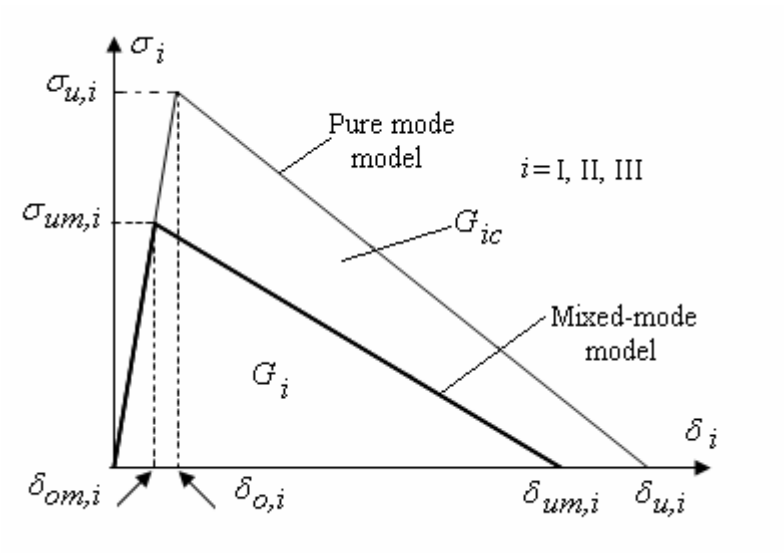

Fig. 2 Pure and mixed-mode damage model.

The G_{IIc} value is calculated from the P-δ-a values obtained numerically. However, considering the experimental difficulties associated to crack measurement during propagation, a new data reduction scheme (Compliance-Based Beam Method – CBBM) proposed by (de Moura, 2006) is applied. The method is based on the specimen compliance and on the crack equivalent concept. Including shear effects, the specimen compliance during crack propagation can be written as,

$$C = \frac{\left(3a_{\text{eq}}^3 + 2L^3\right)}{8E_{\text{f}}Bh^3} + \frac{3L}{10G_{13}Bh}. \tag{3}$$

where $a_{\text{eq}} = a + \Delta a_{\text{FPZ}}$, Δa_{FPZ} being the crack length correction to account for the *Fracture Process Zone* (FPZ) effect. Considering the initial crack length (a_0) and initial compliance (C_0), an estimate of the flexural modulus bending can be obtained by,

$$E_{\text{f}} = \frac{3a_0^3 + 2L^3}{8Bh^3}\left(C_0 - \frac{3L}{10G_{13}Bh}\right)^{-1}. \tag{4}$$

From equations (3) and (4) it can be written,

$$a_{\text{eq}} = \left[\frac{C_{\text{corr}}}{C_{0\,\text{corr}}}a_0^3 + \frac{2}{3}\left(\frac{C_{\text{corr}}}{C_{0\,\text{corr}}} - 1\right)L^3\right]^{1/3} \tag{5}$$

where C_{corr} is given by,

$$C_{\text{corr}} = C - \frac{3L}{10G_{13}Bh}. \tag{6}$$

G_{IIc} can now be obtained from the Irwin-Kies relation,

$$G_{\text{IIc}} = \frac{9P^2a_{\text{eq}}^2}{16B^2E_{\text{f}}h^3}. \tag{7}$$

where a_{eq} and E_{f} are given by equations (5) and (4), respectively. This approach does not require crack length measurements during the tests. On the other hand, the flexural modulus is computed from equation (4), which avoids its determination in separated tests. G_{IIc} only depends on G_{13}=G_{LR}. However it was verified that this parameter does not have much influence on the measured value of G_{IIc} (de Moura, 2006).

Initially, a 3D finite element analysis was performed (Figure 3) using three-dimensional 8-node brick elements from ABAQUS® software and previously developed 8-node interface finite elements (Gonçalves, 2000). The finite element mesh has 30250 brick elements and 4300 interface finite elements. The interface finite elements were placed at the mid-plane of the un-cracked region (detail 1 in figure 3). Opened interface finite elements were defined in the region corresponding to the initial crack to avoid interpenetration of the specimen arms. Contact conditions were imposed to simulate the interaction between the actuator/supports and the ENF specimen (see details 1 and 2 in figure 3). Firstly, the strain energy release rates distributions (G_{I}, G_{II} and G_{III}) at the crack tip and along of the specimen width, were obtained using the Virtual Crack Closure Technique (VCCT) (Rybicki, 1977). For the ENF specimen geometry considered, it was found that the average mode II component (G_{II}) was above of 99.8% of the total strain energy (G_{T}=G_{I}+G_{II}+G_{III}) (see figure 4).

A two-dimensional model was also considered in order to minimize the higher computer time consuming characteristic of the 3D model (see figure 5). The numerical 3D and 2D load-displacement curves were compared and good agreement was obtained (see figure 6). Moreover, it was also verified that both analyses can capture the introduced value of G_{IIc} (see figure 7), which demonstrates the soundness of the proposed model and of the 2D analysis.

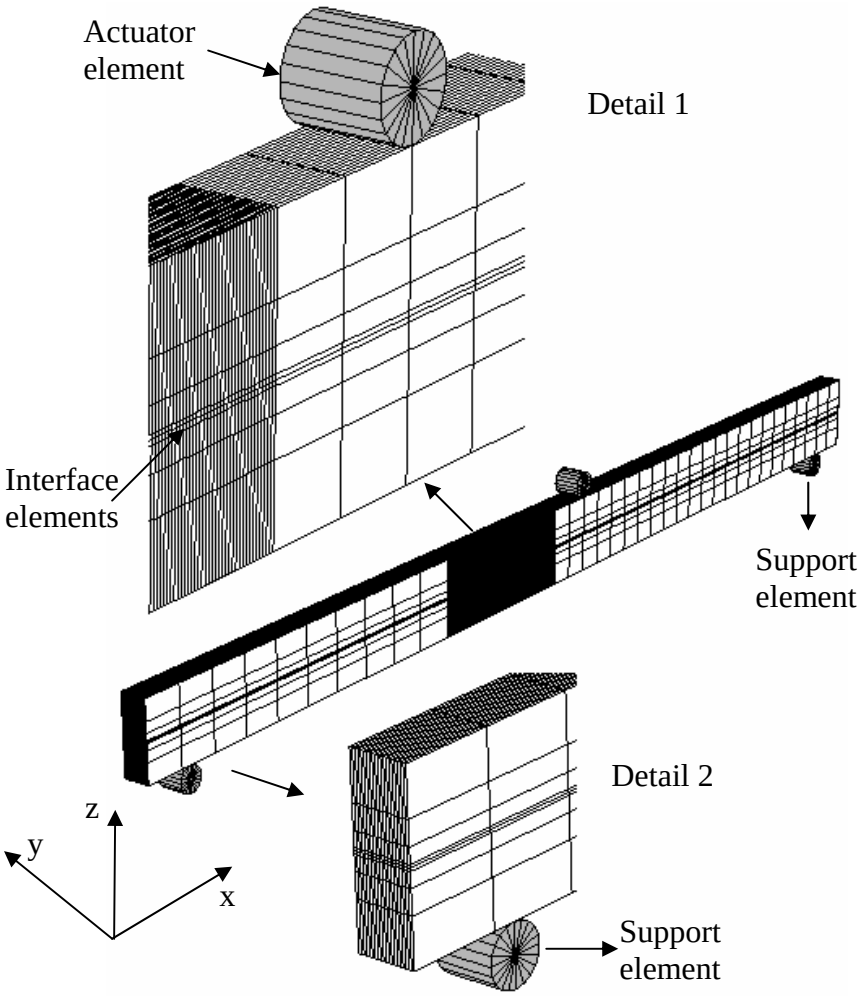

Fig. 3 Mesh used in the three-dimensional finite element model.

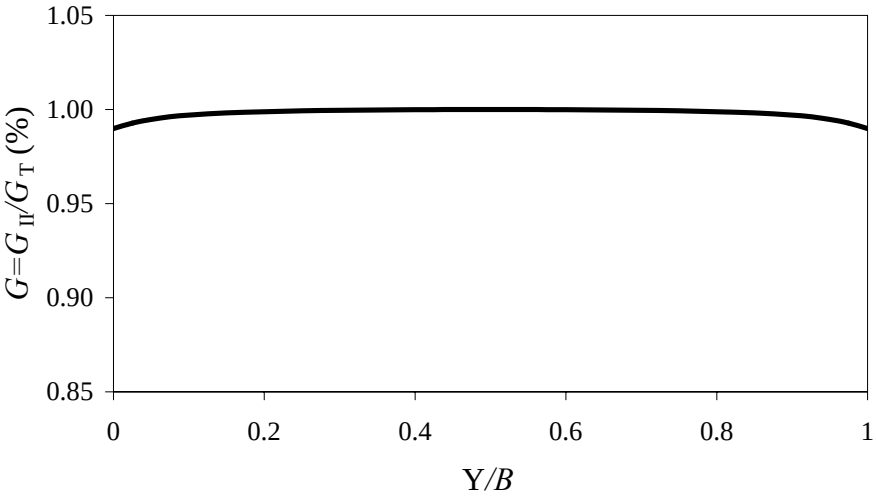

Fig. 4 Distribution of G_{II}, normalized by the total strain energy (G_T), along the normalized width coordinate (B) of ENF specimen.

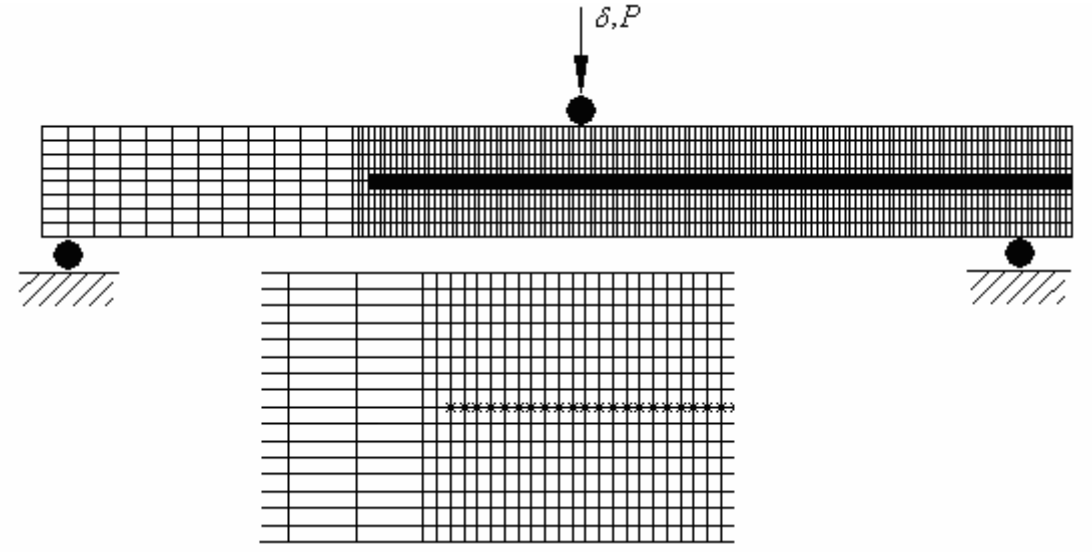

Fig. 5 Mesh of the two-dimensional finite element model.

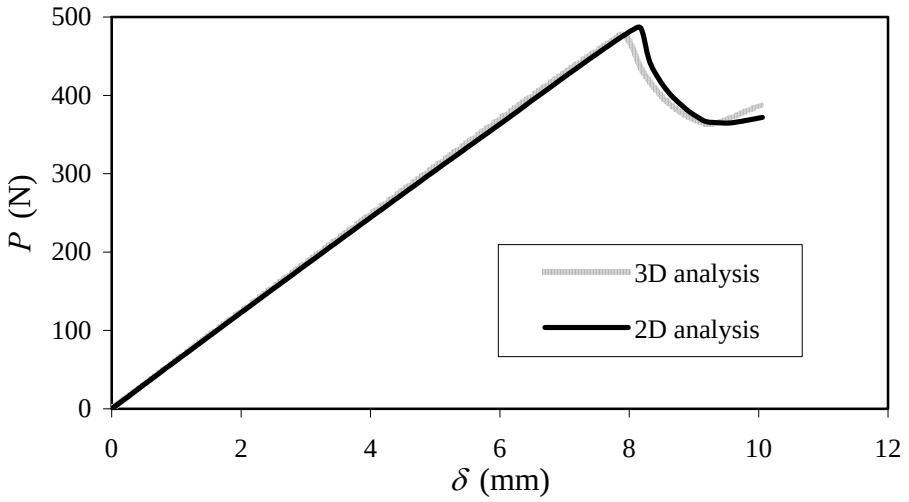

Fig. 6 Comparison between P-δ curves obtained from 2D and 3D approaches.

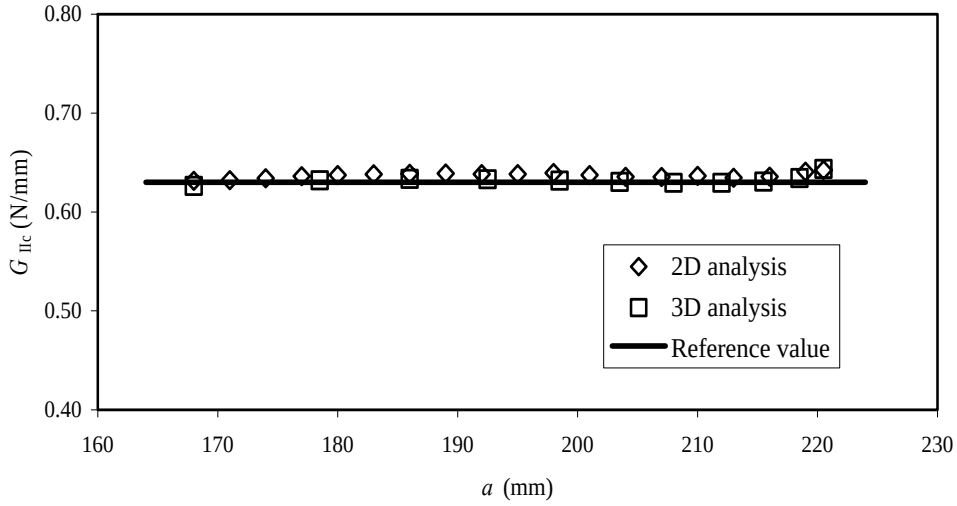

Fig. 7 Comparison between the apparent and inputted G_{IIc}. The straight line corresponds to the inputted value of G_{IIc}.

EXPERIMENTAL TESTS

The *Pinus pinaster* Ait. wood specimens were machined and tested. The material was conditioned in a climate of 20ºC and 65% RH until equilibrium, inducing 12 % moisture content of wood. The average value of specific density of wood was 0.44. The real geometry was recorded for each one of the 24 specimens. The initial crack length, which is a fundamental parameter of the CBBM, was accurately measured using an optical microscope. Two sheets of Teflon film were inserted between the initial crack surfaces in order to minimize the friction effects (see figure 8). The specimen was supported by two cylinders and loaded at the mid-span at a crosshead speed of 5 mm/min. During the fracture tests, the applied load and displacement values were recorded (frequency 5 Hz). The crack length during propagation was not measured. In fact, as it can be verified in figure 9 it is not clearly visible the position of the crack tip. The detail 2 of the figure 9 demonstrates that crack tip passed the vertical black reference line, although almost nothing is perceptible on the material. It can be concluded that conventional data reduction schemes based on crack length measurements can induce remarkable errors on the G_{IIc} values.

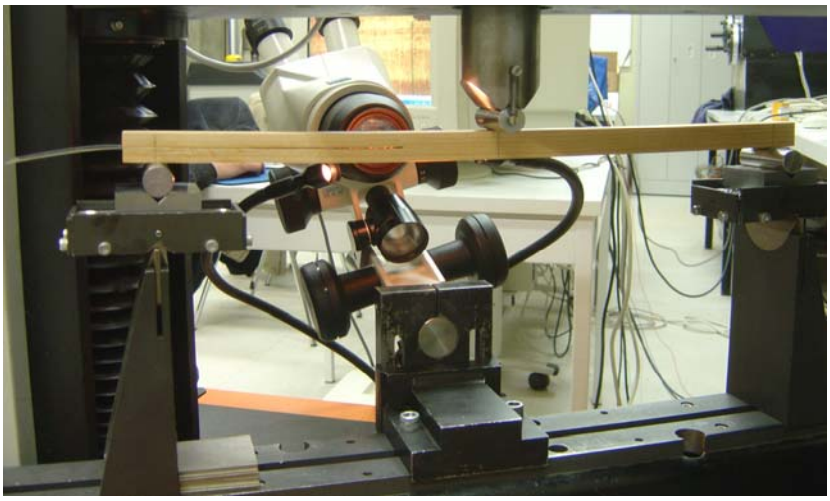

Fig. 8 Experimental setup of the ENF tests.

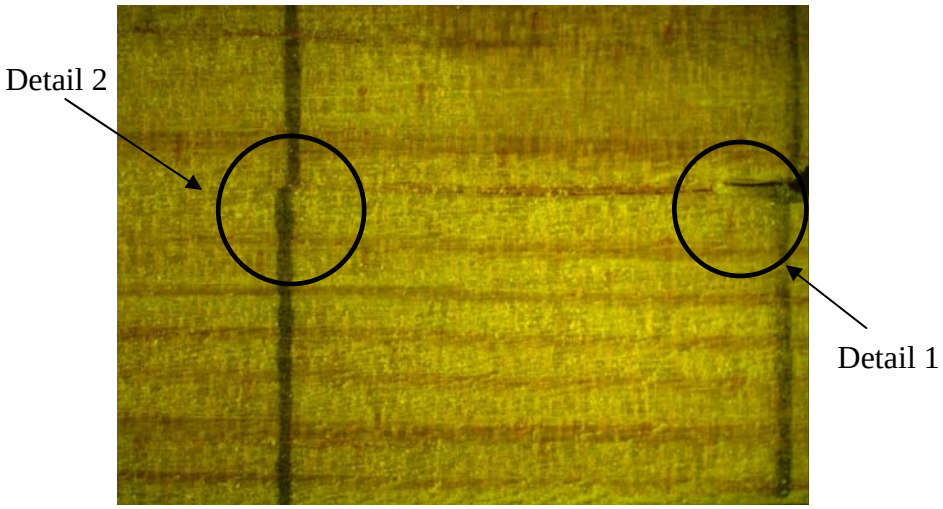

Fig. 9 Microscope image of a crack during the propagation process; Detail 1: Initial crack length; Detail 2: Undefined crack extremity.

Using the proposed CBBM, estimations of experimental initiation and critical values of G_{II} were achieved. Figures 10 and 11 present the P-δ and the R-curves of all tested specimens. Some scatter on initial specimen stiffness can be observed in figure 10, which reveals the modulus variability between different specimens.

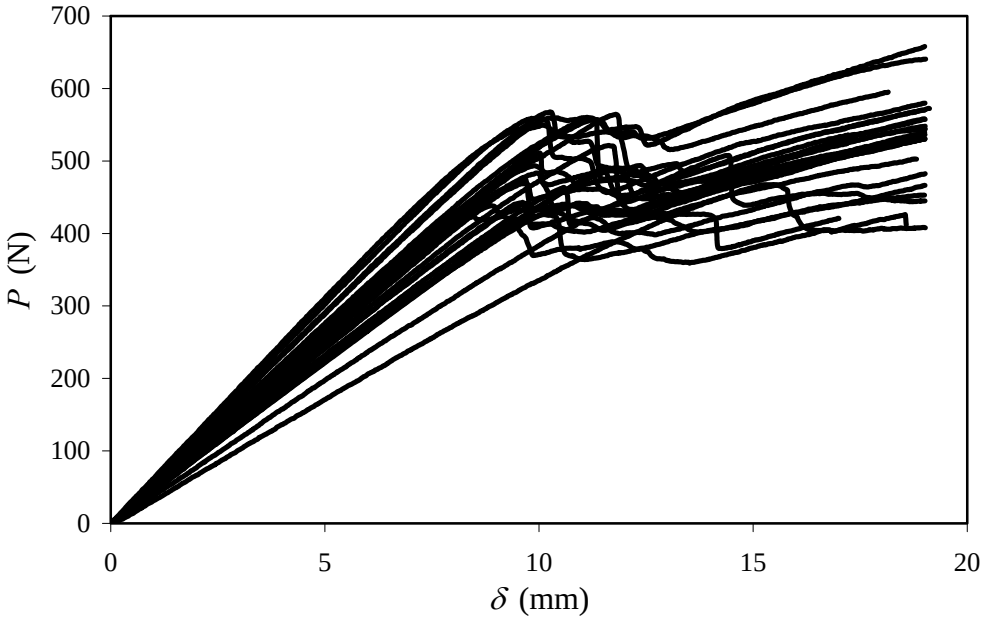

Fig. 10 Experimental P-δ curves.

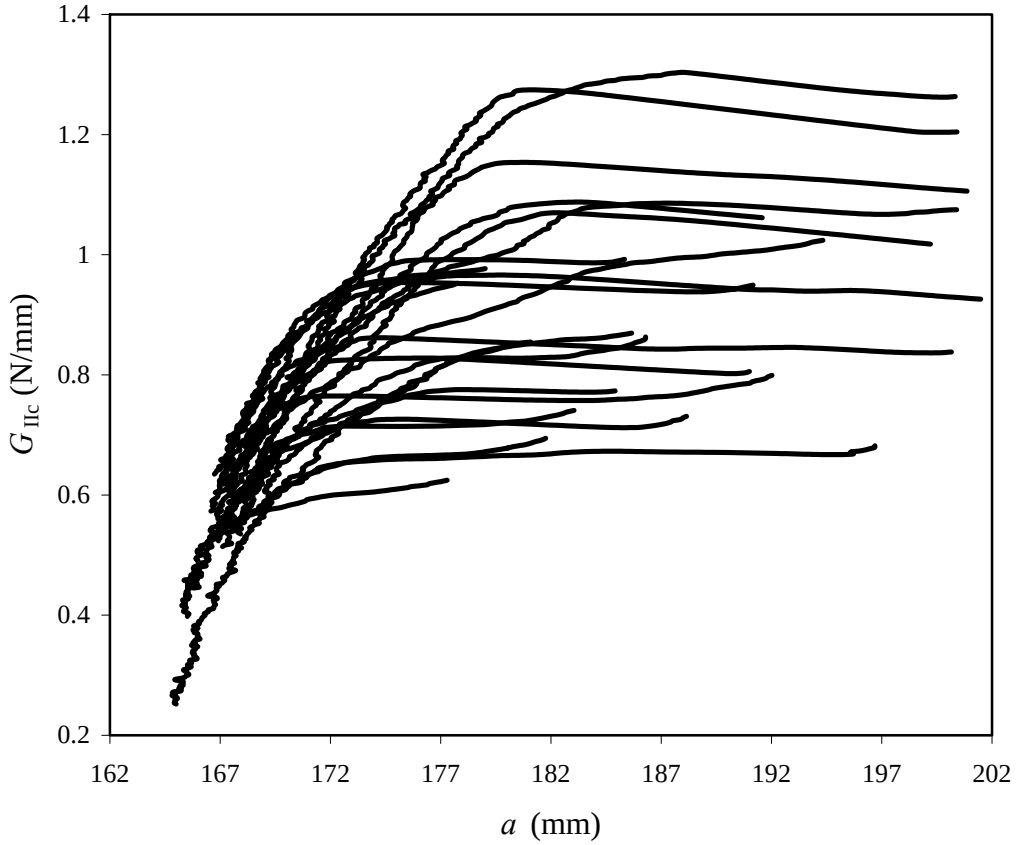

Fig. 11 Experimental R-curves.

Figure 12 shows the different fracture surfaces observed by Scanning Electron Microscopy (SEM). Figure 12 (a) shows the typical pre-crack surface initiated by saw and adjusted by a blade in mode I. The transition between the pre-crack and the mode II propagation surfaces is clearly visible in figure 12 (b). Figures 12 (c-d) present in detail the typical fracture surfaces of mode II propagation.

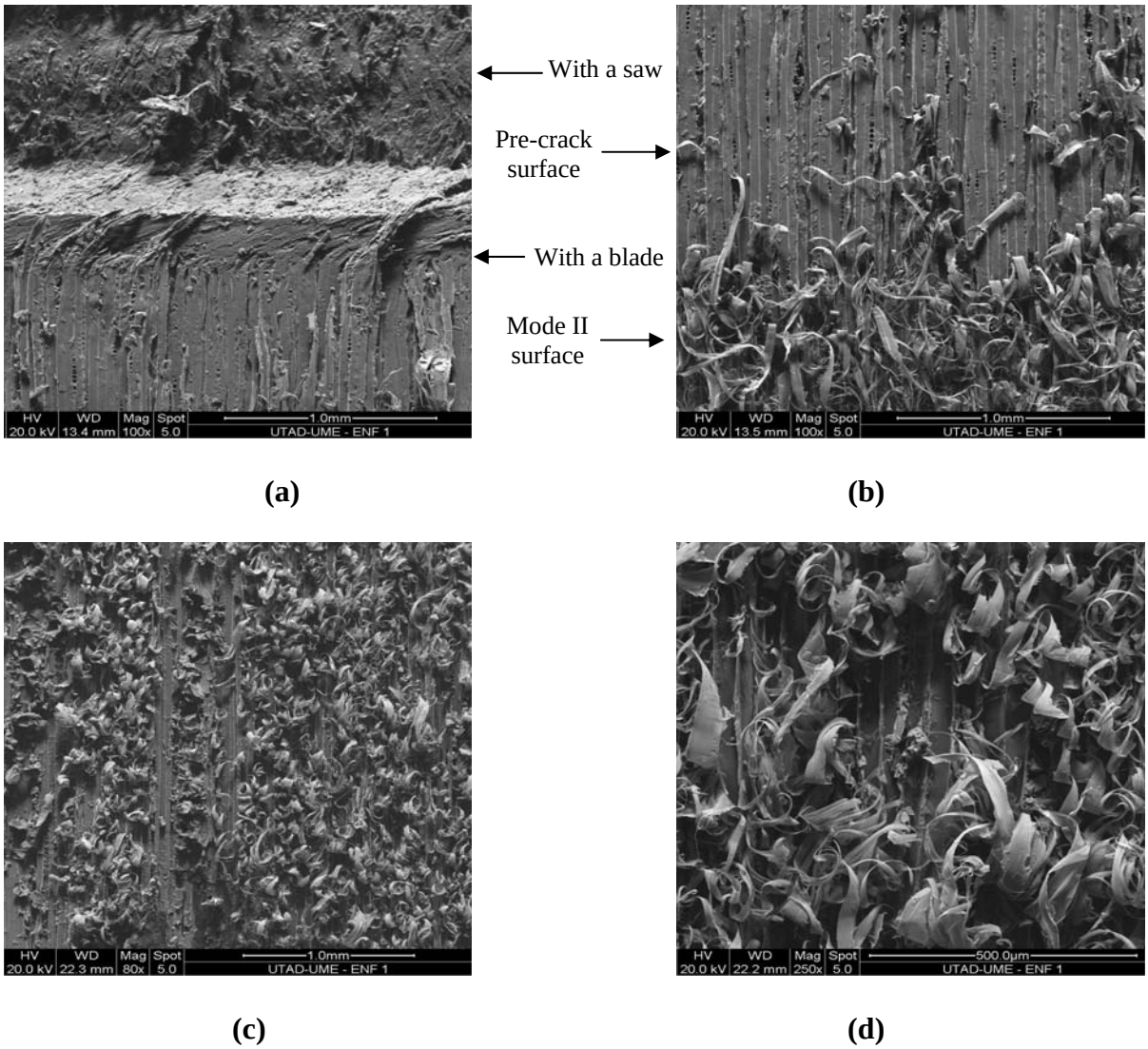

(a) **(b)**

(c) **(d)**

Fig. 12 SEM micrographs: (a) Pre-crack fracture surface (b) Transition between pre-crack and mode II fracture surfaces (c) typical mode II fracture surface (d) detail of mode II fracture surface

RESULTS

In order to verify the applicability of the CBBM all specimens were numerically simulated considering their real dimensions. Figure 13(a) and 13(b) presents typical P-δ and the corresponding R-curve for a given specimen, respectively. The main objective is to compare the numerical and experimental results for the P-δ curves, the G_{IIini} at initiation and its critical value defined by the plateau of the R-curve (see figure 13b). The damage initiation was defined in the P-δ curves as being the point corresponding to the beginning of the nonlinear behaviour. It must be noted that the plateau values (Figure 11) correspond to the inputted G_{IIc} for each specimen in the numerical cohesive model. Figures 14 and 15 show the good agreement obtained in the two analyses. Table 2 summarises the global results for all

specimens. A standard deviation of approximately 20% was obtained for experimental G_{IIc} at the plateau, which can be considered normal in wood. The errors between numerical and experimental values for P_{max}, G_{IIini} and G_{IIc} are lower than 2% which is excellent for wood. Therefore, the present study validates the CBBM for measuring the mode II fracture resistance of wood.

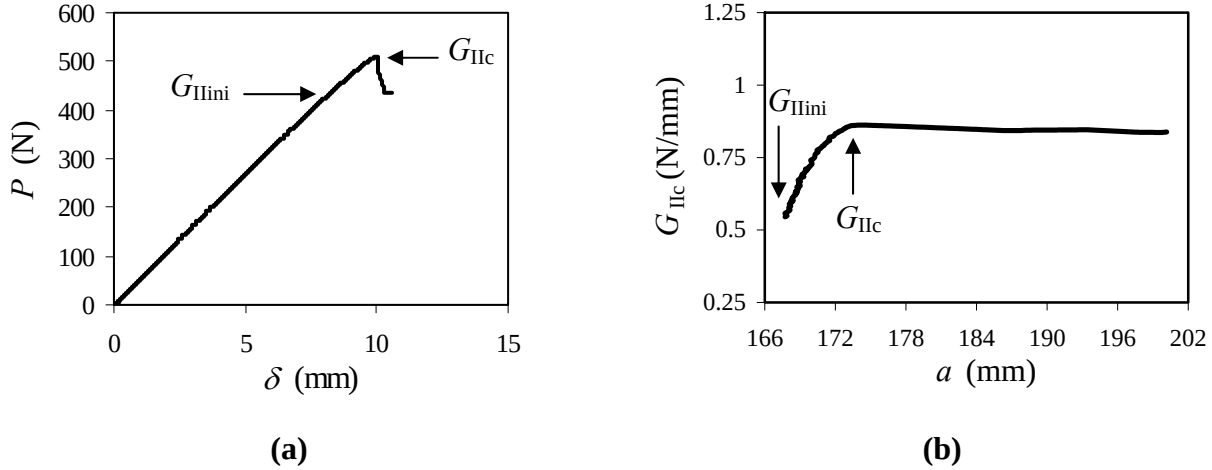

Fig. 13 Typical experimental P-δ curves (a) and R-curves (b) corresponding to specimen 10.

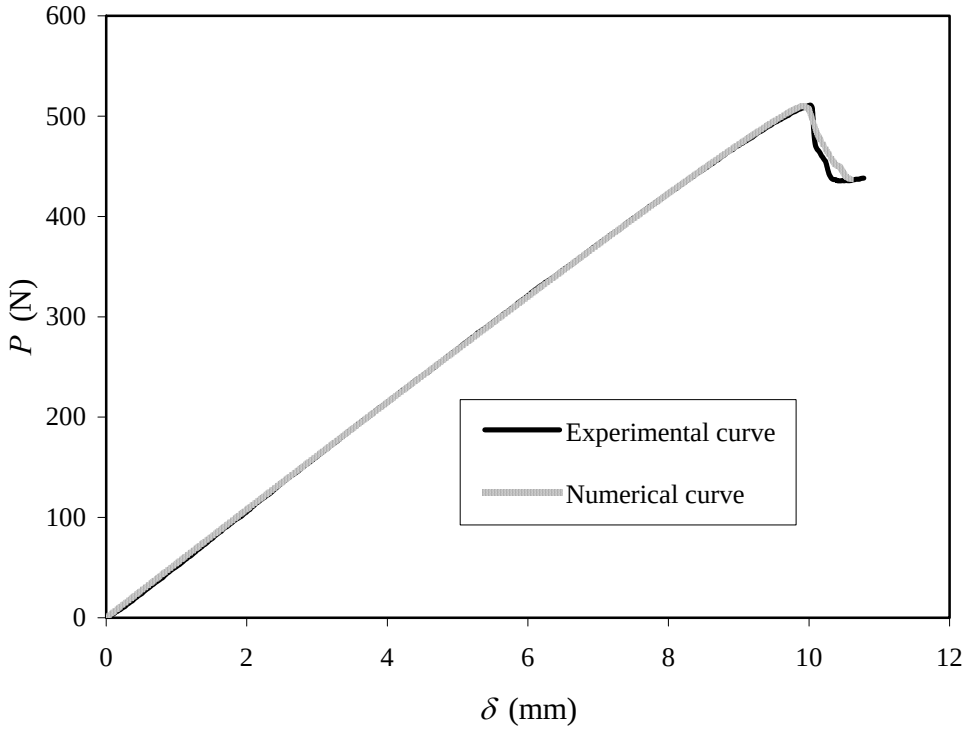

Fig. 14 Comparison between the experimental and numerical P-δ curves of the tested specimen (specimen 10).

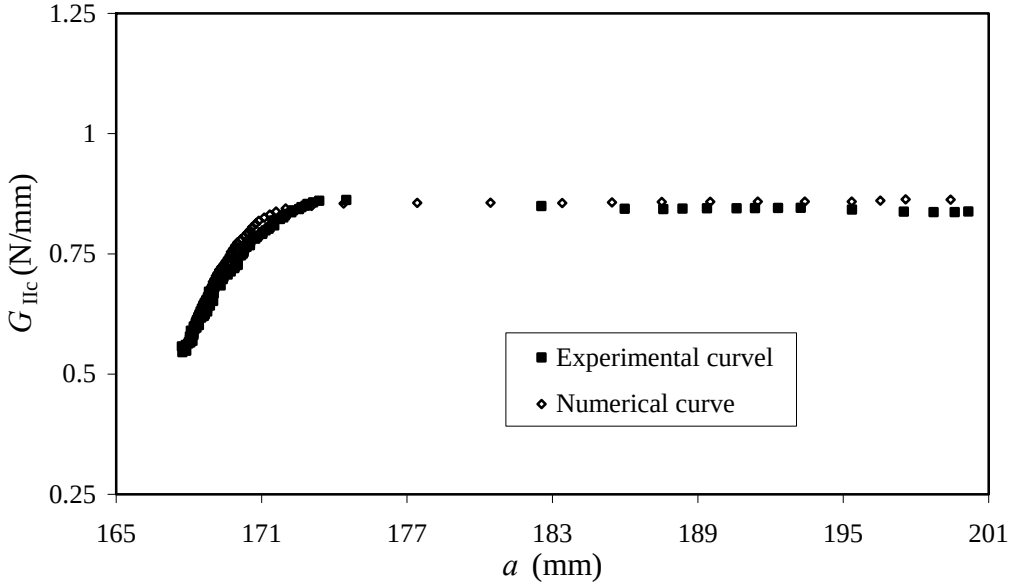

Fig. 15 Comparison between the experimental and numerical *R*-curves of the tested specimen (specimen 10).

Table 2. Summary of the experimental and numerical results for all specimens.

	Experimental results			**Numerical results**			**Error**		
Specimen	$P_{máx}$ **(N)**	$G_{II\ ini}$ **(N/mm)**	G_{IIc} **(N/mm)**	$P_{máx}$ **(N)**	$G_{II\ ini}$ **(N/mm)**	G_{IIc} **(N/mm)**	$P_{máx}$ **(%)**	$G_{II\ ini}$ **(%)**	G_{IIc} **(%)**
1	467.4	0.445	1.273	488.54	0.457	1.265	2.632	-0.572	4.523
2	507.48	0.398	1.262	528.36	0.396	1.248	-0.506	-1.087	4.114
3	564.36	0.635	1.146	579.41	0.635	1.126	0.045	-1.742	2.666
4	469.2	0.579	0.767	475.74	0.573	0.754	-1.028	-1.695	1.393
5	414.36	0.252	0.650	416.33	0.257	0.642	1.981	-1.192	0.476
6	441.36	0.514	0.718	442.33	0.520	0.709	1.050	-1.264	0.221
7	549.48	0.573	0.971	579.35	0.580	0.953	1.158	-1.847	5.436
8	493.68	0.612	1.077	518.09	0.612	1.062	-0.115	-1.352	4.945
9	510.84	0.545	0.860	510.28	0.547	0.844	0.235	-1.831	-0.109
10	463.56	0.604	0.823	464.17	0.612	0.811	1.228	-1.429	0.131
11	483.48	0.524	0.822	492.94	0.528	0.810	0.778	-1.452	1.956
12	423.01	0.537	0.595	425.66	0.537	0.585	0.009	-1.635	0.628
13	536.16	0.618	0.950	536.25	0.619	0.933	0.143	-1.786	0.017
14	521.64	0.550	1.053	536.77	0.552	1.036	0.426	-1.634	2.901
15	438.36	0.535	0.654	440.04	0.539	0.644	0.729	-1.543	0.382
16	567.72	0.740	0.983	566.59	0.742	0.966	0.274	-1.751	-0.200
17	441.96	0.516	0.834	459.31	0.517	0.826	0.053	-1.027	3.925
18	480.84	0.682	0.954	489.59	0.681	0.944	-0.145	-1.043	1.820
19	556.56	0.688	0.941	552.43	0.696	0.927	1.156	-1.568	-0.743
20	474.6	0.685	0.761	472.23	0.686	0.751	0.188	-1.302	-0.500
21	442.92	0.552	0.712	441.12	0.557	0.700	1.003	-1.686	-0.406
22	558.84	0.713	0.929	562.62	0.718	0.913	0.774	-1.748	0.677
23	559.32	0.649	1.078	576.53	0.652	1.064	0.459	-1.315	3.077
24	493.56	0.575	0.837	510.28	0.565	0.823	-1.579	-1.729	3.387
Average values	494.195	0.572	0.902	502.71	0.574	0.889			
St. deviation	9.83	18.71	20.41	10.24	18.57	20.54			

CONCLUSIONS

A Compliance-Based Beam Method (CBBM) based on the equivalent crack concept and specimen compliance is presented. This data reduction method avoids crack length measurements during the experimental tests and additional experiments to obtain elastic properties. The method was used to verify the performance of the ENF test to obtain the real G_{IIc} of wood. Afterwards it was used as a data reduction scheme for the ENF experimental tests. Each specimen was numerically simulated and the numerical and experimental P-δ and R-curves were in good agreement. This conformity between the experimental and numerical results validates the CBBM as a possible standard data reduction scheme to obtain the G_{IIc} value in wood.

REFERENCES

Barrett J.D, Foschi R.O. Mode II stress-intensity factors for cracked wood beams. Engineering Fracture Mechanics, 9; 1977 p. 371-378.

Caumes, P. Rupture d´un matériau anisotropic en conditions polymodales (Le bois), Phd thesis, Université de Bordeaux I., France ; 1987.

de Moura M.F.S.F, Gonçalves J.P.M, Marques A.T, Castro P.M.S.T. Modelling compression failure after low velocity impact on laminated composites using interface elements. Journal of Composite Materials, 31; 1997 p. 1462-1479.

de Moura, M.F.S.F, Silva, M.A.L, de Morais, A.B, Morais, J.J.L. Equivalent crack based mode II fracture characterization of wood. Engineering Fracture Mechanics, 73 (8); 2006 p. 978-993.

Gonçalves J.P, de Moura M.F.S.F, Castro P.M.S.T, Marques A.T. Interface element including point-to-surface constraints for three dimensional problems with damage propagation. Engineering Computations, 17; 2000 p. 28-47.

Jensen J.L. Quasi-non-linear fracture mechanics analysis of the double cantilever beam specimen. Journal Wood Science, 51; 2005 p. 566-571.

Morel S, Mourot G, Schmittbuhl J. Influence of the specimen geometry on *R*-curve behaviour and roughening of fracture surfaces. International Journal of Fracture, 121; 2003 p. 23-42.

Rybicki E.F, Kanninen M. F. A finite element calculation of stress intensity factors by a modified crack closure integral, Engineering Fracture Mechanics, 9; 1977 p. 931–938.

Yoshihara H, Kawamura T. Mode I fracture toughness estimation of wood by the DCB test. Composites Part A: applied science and manufacturing, *in press*.

Yoshihara H, Ohta M. Measurement of mode II fracture toughness of wood by the end-notched flexure test. Journal of Wood Science, 46; 2000 p. 273-278.

Yoshihara H. Mode II *R*-curve of wood measured by 4-ENF test. Engineering Fracture Mechanics, 71; 2004 p.2065-2077.